Conformer Selection Upon Dilution with Water: The Fascinating Case of Liquid Ethylene Glycol Studied via Molecular Dynamics Simulations

Anjali Gaur and Sundaram Balasubramanian*

Chemistry and Physics of Materials Unit

Jawaharlal Nehru Centre for Advanced Scientific Research, Bangalore 560 064, India

E-mail: bala@jncasr.ac.in

Abstract

The aqueous solution of ethylene glycol (EG) is a simple, yet a binary liquid mixture that displays rich conformational and structural behavior, which has not yet been adequately explored through atomistic molecular dynamics simulations. Herein, employing an accurate force field for EG, several physical properties of this solution are calculated to be in quantitative agreement with experimental data. While 79% of molecules in neat liquid EG exist with their central OCCO dihedral in the *gauche* state, this fraction increases to 89% in the dilute aqueous solution, in response to the increase in the static dielectric constant of the solution from that of neat liquid EG. The increase in *gauche* conformers increases the mean dipole moment of EG molecules in the solution which is additionally contributed via specific conformational states of the two terminal HOCC dihedral angles.

Introduction

Water has been used as a coolant in automobile industries since the early 20th century; however, it is not used in its pure form. Rather, anti-freezing agents such as ethylene glycol (EG) and propylene glycol along with corrosion inhibitors are mixed with water.[1–4] Mixing EG with water increases its boiling point and reduces the freezing point, hence providing a wider liquidus range than neat water.[5] Needless to say, physical properties are inherently related to intermolecular interactions; therefore, the water-EG mixture has been studied extensively using various experimental techniques such as Raman,[6] ATR-FTIR,[7] near-infrared (NIR),[8] and sum-frequency generation SFG[9] spectroscopy.

Water and EG are completely miscible[10] at all concentrations of the latter in the aqueous solution. Wang et al. observed considerable changes in the Raman features corresponding to O-H symmetric and O-H asymmetric stretching modes of water at EG volume fraction (V_{EG}) of 0.5. They concluded that EG-water hydrogen bonded structures dominate over water-water clusters at high EG concentration.[6] The EG molecule has one central OCCO and

two terminal HOCC dihedral angles (see Figure S1). The HOCC dihedral is less hindered to rotate as opposed to the OCCO dihedral.[11] In its gas phase, EG adopts a conformation with its central OCCO dihedral in the *gauche* state[12,13] (see Section S1 for nomenclature on conformational states, atom types etc., to be used henceforth). The same is true for crystalline EG as well.[14] However, in its neat liquid state, around 21% of EG molecules have their OCCO dihedral in the *trans* conformation.[11,15,16] Recent Raman spectroscopic studies[6] of aqueous EG solution also showed that the population of *trans* conformers reduces upon dilution of EG. Guo et al. studied the ATR-FTIR spectra of aqueous EG solution over a wide range of mole fraction of EG (x_{EG}), from x_{EG} value of 0.99 to 0.0007.,[7] x_{EG} being the mole fraction of EG in the solution. Combining frequencies obtained from density functional theory (DFT) calculations and ATR-FTIR results and particularly focusing on the skeletal stretching vibration ($\nu_{O-C-C-O}$) and CH_2 rocking vibration, they concluded that between $0.71 > x_{EG} > 0.05$, water molecules interrupt the hydrogen bonds between EG molecules and instead form EG-water network. Further, much of the EG molecules present in the *trans* EG conformation was reported to change to the *gauche* conformation.

After studying the near-infrared spectra of EG-water solutions at various temperatures, Chen et al. also arrived at similar conclusions as Wang et al.[6] and Guo et al.,[7] that EG-water association is preferred over that of water-water at less than 50 weight % water content.[8] They also inferred that in EG-water mixtures, water molecules cluster around EG, and that the size of the cluster is proportional to the amount of water.

Apart from spectroscopy, theoretical methods such as classical molecular dynamics and quantum chemical calculations have also been employed to obtain a molecular level understanding of EG-water mixtures at various compositions.[17–25] Cramer and Truhlar carried out quantum chemical calculations of all conformers of EG both in gas and in implicit water phases.[25] The fraction of *trans* conformer of EG in the aqueous medium was estimated to be around 12 %. Chaudhari and Lee studied EG-water$_n$ (n = 1-3) clusters using DFT. They reported that a water molecule bridging the two hydroxyl groups of an EG molecule as the

most stable configuration.[24] Kumar et al. also carried out DFT calculations on EG_m-$water_n$ (m = 1–3, n = 1–4) clusters and reported that the EG dimer consists of two to three hydrogen bonds and that the addition of two water molecules (EG_2-$water_2$) breaks one of the EG-EG hydrogen bond.[22] Using localized molecular orbital energy decomposition analysis, they concluded that EG-water interactions dominate over EG-EG and water-water interactions.

Classical molecular dynamics (MD) simulations have been performed using various force fields to study the dynamics and physical properties of the liquid EG-water binary mixture. Gubskaya and Kusalik used the OPLS-UA[26] force field to study structural aspects of this solution using radial and spatial distribution functions (RDFs and SDFs). They reported a sudden increase in the population of *trans* conformers at $x_{EG} = 0.03$ from 0 % to 56 %, which is not in accordance with available spectroscopic and quantum chemical results discussed earlier.[21] de Oliveira and Freitas studied the structural and thermodynamic properties using three OPLS-AA based force fields.[20] Kaiser et al. examined dynamical properties to understand EG-water dielectric spectra using the OPLS-AA-SEI-M[20] force field. However, at ambient conditions, the translational diffusion coefficient and dielectric constant calculated using the same force field for pure EG is 1150% and 89% away, respectively, from the experimental values.[18] Geerke and Gunsteren developed two non-polarizable (G04 and G05) and three polarizable (COS/E10, COS/E08, and COS/E06) united atom FFs to reproduce solvation free enthalpy of argon in EG-water mixture and physical properties of pure EG liquid.[23] While their non-polarizable FFs predicted dielectric constant more accurately, the polarizable FF COS/E10 predicted diffusion coefficient more accurately. A recently developed GAFF[27] based force field parametrized by us (FF-v1)[16] provides the best agreement with various experimentally measured physical properties of neat EG. The translational diffusion coefficient of EG was calculated to be just 5% higher while the dielectric constant was 35% lesser than the experimental values.[16] To the best of our knowledge, except for FF-v1, none of the force fields reproduces experimentally reported dynamical properties of EG well. In particular, FF-v1 is the only force field for EG which reproduces the conformer populations

correctly in accordance with both experiment and ab initio MD simulation results. Hence, we felt it important to investigate EG-water solutions using this newly developed force field, FF-v1.[16]

Physical properties of the solution such as density, translational self-diffusion coefficient, and static dielectric constant at four different mole fractions of EG (x_{EG} = 0, 0.3, 0.5, 0.8) calculated here are in excellent agreement with experimental data. We also report an interesting behavior in the population of *trans* conformers of EG, with increasing concentration of water. The variation of static dielectric constant of the solution with EG concentration is explained through the change in the distribution of molecular dipole moment of EG, which is impacted more by *gauche* conformers than the *trans* ones.

Computational Details

Equilibrium Molecular Dynamics Simulations

Classical MD simulations at several compositions of EG-water binary mixtures in the liquid phase (see Table S1) were carried out using GROMACS-2020.4[28–30] software. For each composition, a cubic box of side length approximately 51Å was packed with EG and water molecules, using PACKMOL,[31] at the density reported experimentally. All the EG molecules were present in the *gauche* conformation in all these initial configurations. A GAFF[27] based FF proposed recently by our group was used for EG[16] and the SPC/E[32] model was used to represent water. Lorentz-Berthelot combination rules were used to compute cross Lennard-Jones (LJ) and Coulomb interactions. 1-4 LJ and Coulomb interactions were scaled by 0.5 and 0.8333, respectively. A cutoff radius of 10Å was used for short-range interactions with an additional 2Å buffer to update the pair list every ten steps using the Verlet cutoff[33] scheme. Energy and pressure corrections were applied. Long-range Coulomb interactions were calculated using the particle mesh Ewald[34] method with interpolation order of 4 and 0.12nm grid spacing and a relative tolerance of 10^{-5}. The equations of motion were integrated

using leap-frog integrator with a time step of 1fs. All the covalent bonds involving hydrogen atoms were constrained using LINCS[35] algorithm. Temperature and pressure were controlled using Nosé-Hoover[36,37] thermostat and Parrinello-Rahman[38] barostat, respectively. The temperature and pressure coupling time constant were 1ps and 10ps, respectively.

Well-tempered Metadynamics Simulation

Gromacs-2020.4[30] patched with PLUMED-2.6.2[39] was used to perform the well-tempered metadynamics[40] simulation (WTMetaD). System details are presented in Table S7. Before starting the WTMetaD simulation, a 25ns long NPT simulation at 298.15K and 1 bar followed by a 50ns NVT run were performed at the average density to equilibrate the system. The WTMetaD simulation was performed to obtain the free energy profile of the OCCO dihedral angle of one EG molecule soaked in a water bath. Hence, the OCCO dihedral angle was chosen as the collective variable (CV). WTMetaD simulation parameters are presented in Table S8. Preliminary convergence of the WTMetaD simulation was checked by observing the CV and Gaussian hill height as a function of simulation time (See Figure S8a and S8b). Convergence of free energy was confirmed by performing error analysis using the block averaging method (See Figure S8c).

Results and Discussion

Physical Properties

Density and static dielectric constant of the solution, and the molecular translational self-diffusion coefficients were calculated at four different EG mole fractions (x_{EG}). These physical properties as a function of x_{EG} are displayed in Figure 1. Density was calculated from the last 5ns of a 25ns NPT simulation at various mole fractions of EG (x_{EG}) and compared against experimental[41] data (Figure 1a). While the predicted density values are lower than the experimental data at all x_{EG} except at $x_{EG} = 0.0$, the maximum deviation is

just -1.4%. Six independent NVT simulations were performed to calculate the translational self-diffusion coefficient (D_{self}) and the cross correlations between the diffusing species have not been considered. Each simulation was 50ns long, and the initial 5ns segment of the trajectory was discarded for equilibration. D_{self} for EG and water was calculated using the Einstein relation (see Section S5) by carefully choosing the diffusive regime (see Figure S5). D_{self} for both EG and water are in remarkable agreement with experimental[42] data (Figure 1b). The largest deviation of 14.3 % is seen in the D_{self} for pure water. Water has a higher diffusion coefficient at all the compositions than EG because of its lower molecular mass; however, its water diffusion coefficient reduces drastically in the range $x_{EG} = 0$ to $x_{EG} = 0.3$. This observation suggests that the motion of water molecules is hindered just by mixing a small amount of EG; Loskutov and Kosova[44] also reported a drastic increase in viscosity from 1.2cP at $x_{EG} = 0.01$ to 5.46cP at $x_{EG} = 0.31$ (Table 2 of Ref. 44). Mixing EG with water also affects dielectric polarization. The dielectric constant of the solution monotonously increases with decrease in the amount of EG.[43] We calculated the dielectric constant using six independent MD runs at every composition, each 50ns long and compared them with experimental[43] data (Figure 1c). The largest deviation of -35.5% in dielectric constant is seen

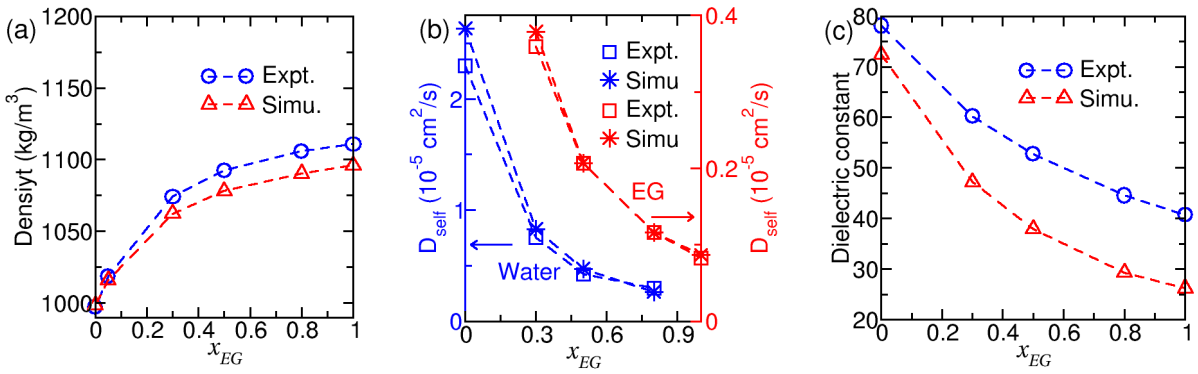

Figure 1: (a) Density (b) Translational self-diffusion coefficient (D_{self}), and (c) Dielectric constant calculated at various mole fractions of EG (x_{EG}) at 298.15 K and 1 bar. Experimental data for density, self-diffusion coefficients, and static dielectric constant are taken from Refs. 41, 42, and 43, respectively. Maximum deviation are -1.3%, 14.3%, -35.1%, respectively. Numerical values of these quantities and error on the mean are presented in Tables S4, S5, and S6, respectively. Error bars are smaller than the symbol size, hence are not shown.

for pure EG. Nevertheless, the behavior of the calculated dielectric constant as a function of x_{EG} matches that seen in experiments. The increase in dielectric constant of the solution alters the conformer population of EG molecules, as discussed in the upcoming sections.

For pure EG, isothermal compressibility (β_T) and thermal expansion (α_P) were also calculated from last 10ns of an 25ns NPT run at 298.15 K and 1 bar using volume fluctuations.[45] The 10ns trajectory was divided in five equal parts to calculate standard error. A comparison of computed β_T and α_P with experimental values is presented in Table 1. Although the FF-v1 force field was not refined to reproduce β_T and α_P, the comparison between simulated and experimental results is decent. A precise evaluation of these values from simulations would require much larger system sizes (5000 molecules as in Ref. 46) than employed herein.

Table 1: A comparison of isothermal compressibility (β_T) and thermal expansion (α_P) of neat liquid EG calculated using simulations with experimental values.

Property	Simulation	Expt.
β_T x 10^{-5} bar^{-1}	4.72 ± 0.17	3.34[47]
α_P x 10^{-4} K^{-1}	9.34 ± 0.12	6.7[48]

Radial Distribution Functions

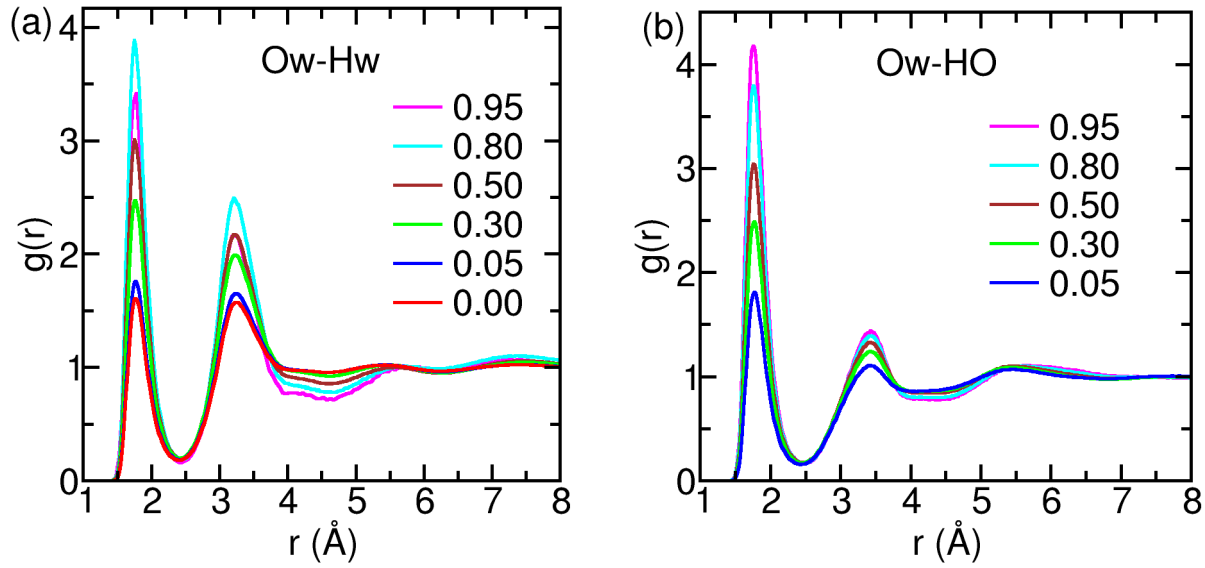

Figure 2: Intermolecular radial distribution function between oxygen atoms of water molecules (Ow) and (a) hydrogen atoms of other water molecules (Hw) (b) hydroxyl hydrogen atoms of EG molecules (HO). Legends represent mole fraction of EG.

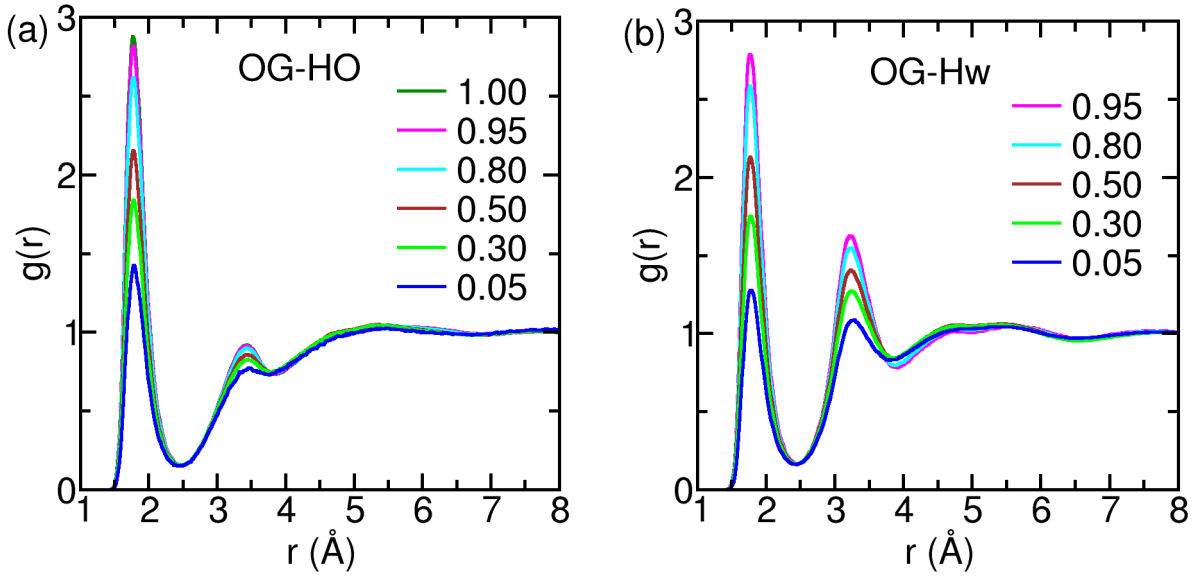

Figure 3: Intermolecular radial distribution function between oxygen atoms of EG molecules (OG) and (a) hydroxyl hydrogen atoms of EG molecules (HO) (b) hydrogen atoms of other water molecules (Hw).Legends represent mole fraction of EG.

EG and water are completely miscible and both possess hydrogen bonding donor and acceptor sites.[49] As discussed in the Introduction, many spectroscopic studies have reported the

presence of hydrogen bonds between EG-EG, EG-water, and water-water in EG-water binary mixtures. Hence, we calculated radial distribution functions (RDFs) related to intermolecular hydrogen bonding, as shown in Figures 2 and 3. The first coordination shell peak position, its minimum, and the coordination number calculated from the RDFs are presented in Table 2. The first peak, corresponding to the most probable hydrogen bond distance, is between 1.7 and 1.8 Å for EG-EG, EG-water, and water-water pairs. A comparison of the peak heights of the Ow-HO and OG-HO g(r)s is in order. At x_{EG}=0.95, wherein the water mole fraction is low, the height of the first peak of Ow-HO g(r) is much larger than that of OG-HO g(r) when x_{EG}=0.05. This implies that water molecules have a higher propensity to hydrogen bond with the hydroxyl hydrogens of EG when the water amount is low, whereas EG, at the same corresponding low amount is unable to do so to the same extent. The same conclusion can be drawn by a comparison of Ow-Hw and OG-Hw g(r) first peak heights at x_{EG}=0.95 (former) and at x_{EG}=0.05 (latter). Thus, at low water contents, water is likely to cluster around each other, such clusters solvated by EG, as pointed out earlier by Kusalik and coworkers[21] and confirmed via oxygen-oxygen RDFs as well (Figure S3).

Table 2: The first shell coordination number (C.N.) representing intermolecular hydrogen bonds at several mole fractions of EG, x_{EG}.

x_{EG}	Ow-Hw	Ow-HO	OG-HO	OG-Hw
1.00	-	-	0.97	-
0.95	0.06	1.31	0.94	0.05
0.80	0.29	1.13	0.82	0.21
0.50	0.77	0.78	0.58	0.59
0.30	1.17	0.50	0.38	0.89
0.05	1.75	0.09	0.08	1.38
0.00	1.89	-	-	-

Fortes and Suard reported the crystal structure of EG-water mixture measured at a temperature of 210 K at $x_{EG} = 0.5$.[50] They reported hydrogen bond distances of 1.7 to 1.8 Å

between EG and water. The hydrogen bond distance obtained herein compares very well with corresponding values in the crystal structure. The coordination number of water hydrogen atoms (Hw) around water oxygen atoms (Ow) and EG oxygen atoms (OG) increases with increase in the mole fraction of water. In contrast, the same for hydroxyl hydrogen atoms (HO) around Ow and OG atoms decreases (See Table 2). RDFs and first shell coordination number between oxygen atoms of EG and water at various mole fractions of EG are presented in SI (Figure S3 and Table S2). The change in the oxygen-oxygen first shell coordination number as a function of x_{EG} is also shown in Figure 4. Note that the coordination numbers in the Figure are per oxygen atom. At the equimolar composition, although both EG's OG and water's Ow are both prima facie on equal grounds for other molecules to interact with, Ow is able to hydrogen bond with more partners as it has two donor sites (i.e., two Hw atoms), while EG's OG has only one, being a hydroxyl group. This conclusion can be drawn from the values of the coordination numbers presented in Table 2, as well as from Figure 4.

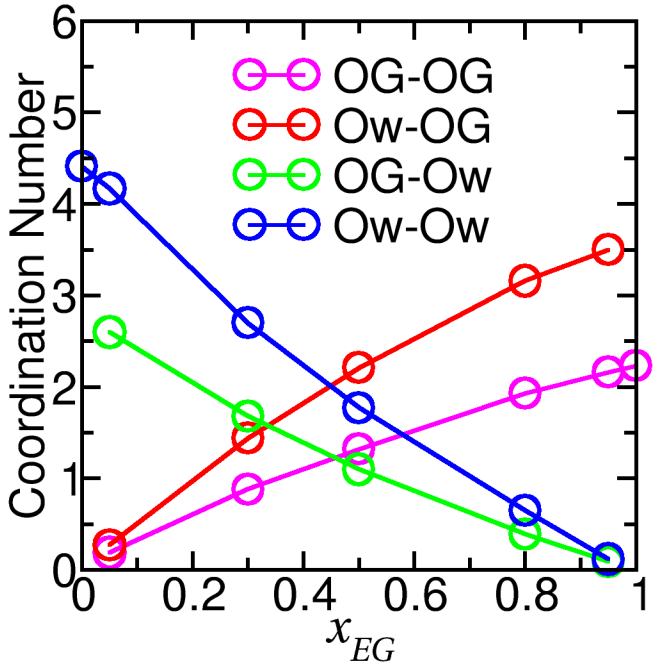

Figure 4: Various oxygen-oxygen coordination numbers as a function of mole fraction of EG (x_{EG}).

Population of EG Conformers: Compositional Dependence

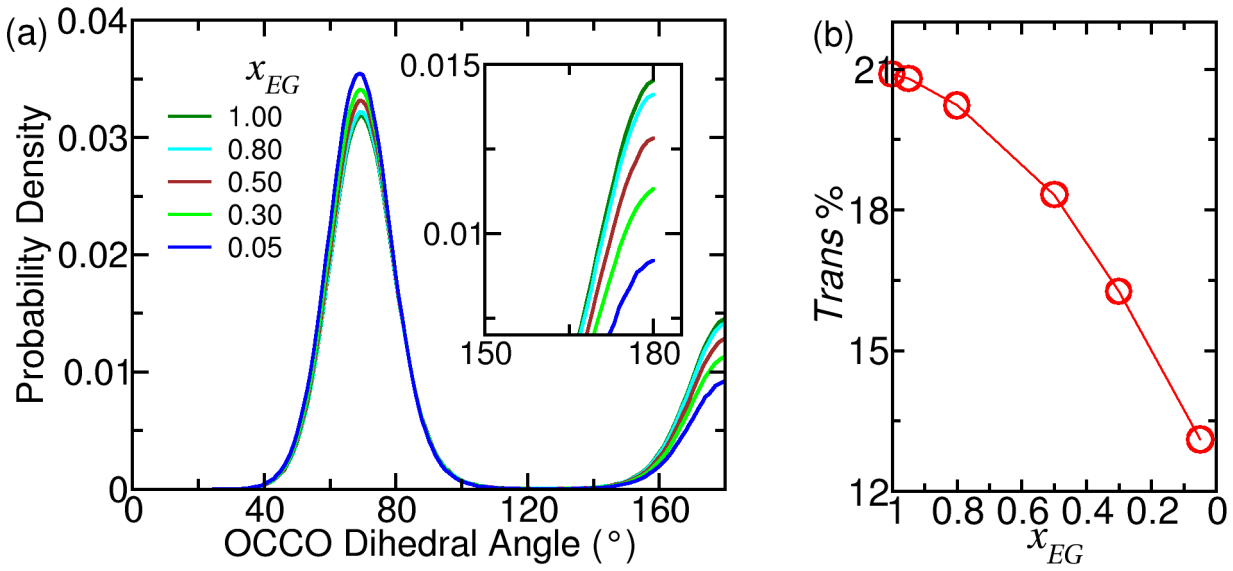

Figure 5: a) Distribution of OCCO dihedral angle of ethylene glycol (EG) at various mole fractions of EG (x_{EG}) in aqueous EG solution. The probability density was calculated by dividing probability with bin width. b) Fraction of conformers in the *Trans* state of the OCCO dihedral of EG as a function of x_{EG}. Line connecting the data points in panel (b) is a guide to the eye.

Several spectroscopic studies and quantum chemical calculations have shown that the population of EG molecules with their central OCCO dihedral in the *trans* conformation reduces upon dilution of liquid EG with water.[6,7,25] Using Raman spectroscopy, Wang et al.[6] showed that the intensity of the peak at 2728 cm^{-1}, which is attributed to this *trans* conformation decreases with increasing amounts of water in the solution, indicating a reduction in the population of the *trans* conformer. Guo et al.,[7] using FTIR-ATR spectroscopy, showed that the ratio of the area of bands corresponding to *trans* and *gauche* conformers ($A\nu_{O-C-C-O-T}/A\nu_{O-C-C-O-G}$) decreases with increasing water concentration, once again pointing to a reduction in the *trans* population. *However, to the best of our knowledge, this fascinating phenomenon has not been reproduced so far in any empirical force field based MD simulation.* The distribution of OCCO dihedral angles at various mole fractions of EG are shown in Figure 5a and the population of *trans* conformers in Figure 5b. In neat liquid EG,

the *trans* conformer fraction is 21%, which is seen to monotonously reduce upon dilution of EG with water. The *trans* population at the lowest concentration studied here ($x_{EG} = 0.05$) is 13.1%.

Cramer and Truhlar[25] calculated the *trans* percentage using implicit solvent quantum chemical calculations and reported a value of 12% in water. We performed WTMetaD simulation of 1 EG molecule in a bath of 4496 water molecules to mimic the dilute aqueous conditions. The collective variable was the OCCO dihedral angle. The free energy difference between the *gauche* and *trans* states of one EG molecule soaked in liquid water is 3.5 kJ/mol, which is around twice the same in neat liquid EG. This free energy difference corresponds to a *trans* population of 10.9%. Our empirical force field based MD simulation results are thus in accordance with the results reported by spectroscopic observations and quantum chemical calculations. In the subsequent section, we shall examine the reasons underlying the variation in the *trans* population with the mole fraction of EG in the aqueous EG solution.

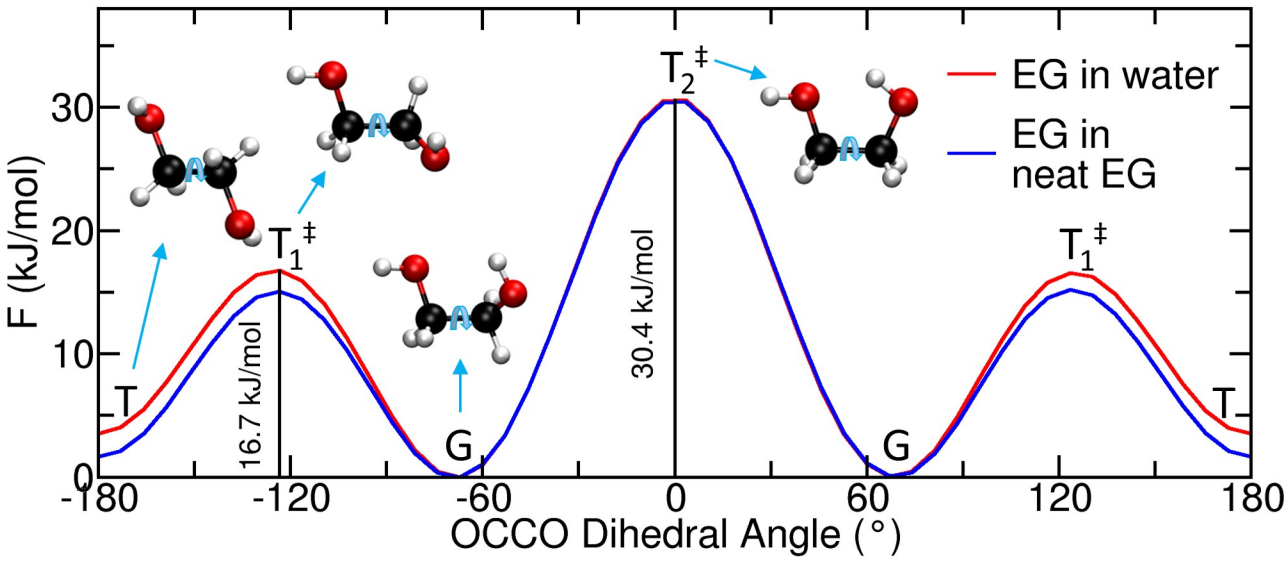

Figure 6: Free energy (F) profile as a function of the OCCO dihedral angle of EG in a dilute aqueous EG solution and in neat EG obtained using well-tempered MD simulations. The free energy difference between *trans* and *gauche* conformers (F(T) - F(G)) in dilute aq. EG solution is 3.5 kJ/mol and that in neat EG is 1.7 kJ/mol.

Distribution of Molecular Dipole Moment of EG

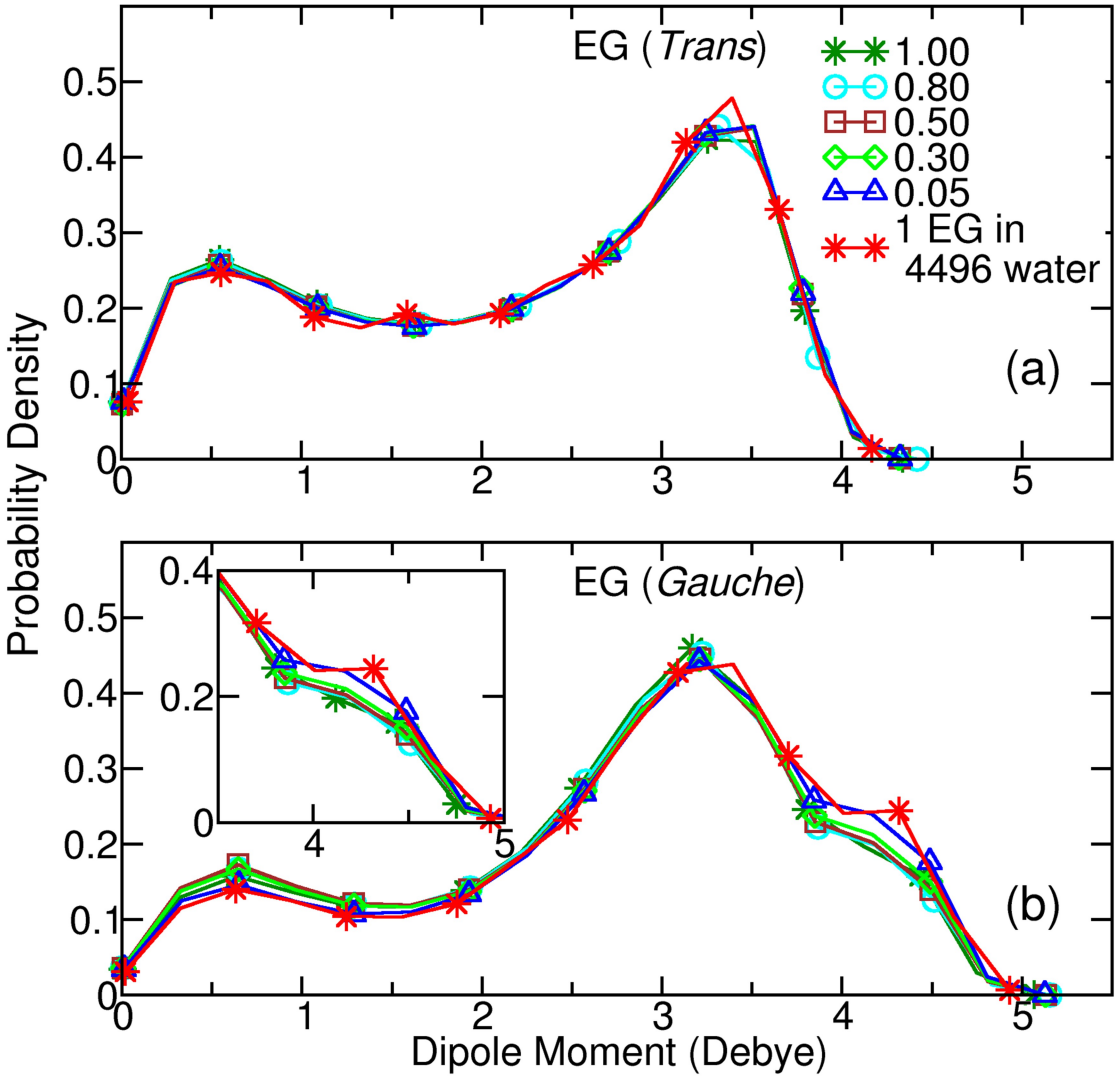

Figure 7: Dipole moment distribution for EG molecules which are in (a) *trans* conformation and (b) *gauche* conformation at various mole fractions of EG (x_{EG}). Inset in (b) shows the same data as the main panel, but highlights the increase in population of higher dipole moment conformers with decrease in x_{EG}. Symbols are shown at every alternate data point for clarity and lines are drawn as a guide to the eye.

In general, the *trans* conformer of EG tends to have a lower dipole moment than the *gauche* conformer.[25] Thus, the reduction in OCCO *trans* fraction with increase in water content has been attributed to the higher dielectric constant of water than that of liquid EG.[6] However, as noted by Jindal and Vasudevan, not all OCCO *trans* conformers have zero dipole moment;

the molecule's dipole moment is also dependent on the conformational state of the two HOCC terminal dihedrals.[51] We calculated the dipole moment distribution of EG molecules with their central OCCO dihedral present in either the *trans* or the *gauche* state as a function of EG concentration in the aqueous solution, and the same is displayed in Figure 7. Most *trans* conformers have a high dipole moment (around 3.5 Debye). Furthermore, there is no significant change in the *trans* EG dipole moment distribution with change in x_{EG}. However, the *gauche* EG dipole moment distribution shows a non-negligible shift to the right increase in dipole moment while going from $x_{EG} = 1.0$ to $x_{EG} = 0.05$, particularly in the higher dipole moment range. The mean dipole moment for *trans* EG, *gauche* EG, and for all the EG molecules (irrespective of the conformational state of the OCCO dihedral) at all the compositions are presented in Table 3.

Table 3: Mean dipole moment of EG molecules which are present in either *trans* and *gauche* conformational states, and the mean dipole moment of all the EG molecules, irrespective of conformation at various mole fractions of EG (x_{EG}).

x_{EG}	Mean Dipole Moment (Debye)		
	Trans EG	*Gauche* EG	EG
1.00	2.31	2.85	2.73
0.80	2.32	2.83	2.72
0.50	2.33	2.82	2.73
0.30	2.34	2.85	2.77
0.05	2.34	2.93	2.86
0.00	2.36	2.96	2.88

The shift in the dipole moment distribution of *gauche* EG towards larger dipole moment values is in response to an increase in the static dielectric constant of the medium, from a value of 41 in neat liquid EG to a value of 78 in neat liquid water. This increase not only increases the fraction of *gauche* conformers (in the central dihedral), but also enhances the access of conformational states in the terminal dihedral angles with large dipole moment values (vide infra).

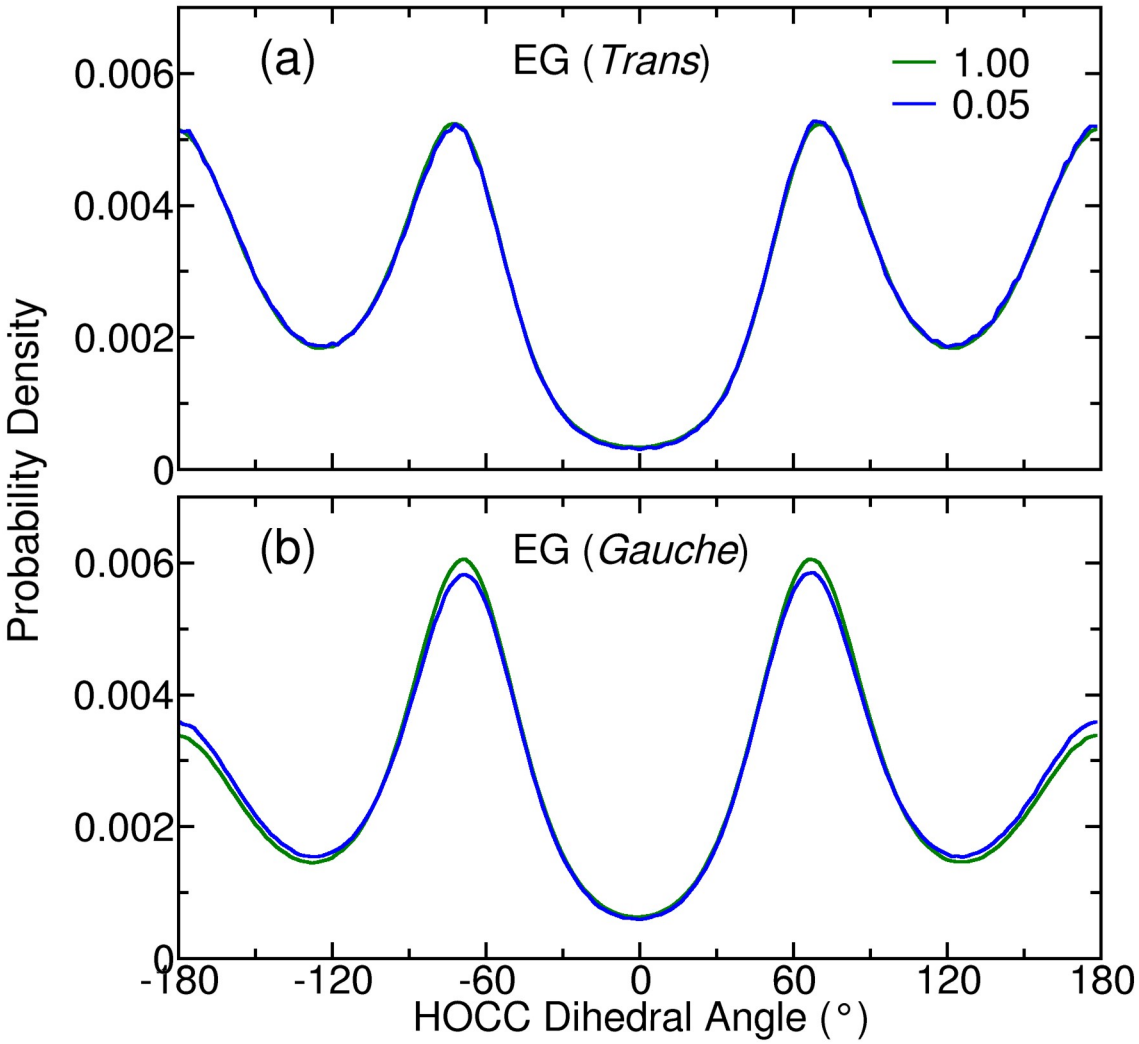

Figure 8: Terminal HOCC dihedral distribution of EG molecules in *trans* and *gauche* conformations. Legends represent mole fraction of EG. The central OCCO dihedral distribution of EG molecules in *gauche* and *trans* conformations do not change with x_{EG} and are shown in SI (Figure S9). The probability density was calculated by dividing probability with bin width. The error on the mean of the distribution is nearly the same as the line width.

The change in the *gauche* EG dipole moment distribution is also reflected in the HOCC (terminal) dihedral distribution of *gauche* EG molecules (Figure 8b). In contrast, the same for *trans* EG molecules remains unchanged throughout the range of EG-water mixture composition, as shown in Figure 8a. No significant change was seen in the OCCO (central) dihedral distribution of both *gauche* and *trans* EG molecules throughout the range of EG-water mixture composition (see Figure S9). The HOCC dihedral distribution of *gauche* EG molecules

exhibits a decrease in probability from ±50° to ±90° and an increase in probability from ±120° to ±180° with increase in water concentration. (Figure 8b). To understand these changes, we calculated the dipole moment of an isolated EG molecule whose OCCO dihedral angle is either 64°(i.e., *gauche*) or 180°(i.e., *trans*), as a function of both its HOCC (terminal) dihedral angles, using site charges of our force field. The same is shown in Figure 9. Some of the *gauche* EG conformers have much higher dipole moment than the *trans* EG conformers. For the *gauche* EG conformer, regions of highest dipole moment, shown in yellow, occur either when both the HOCC dihedral angles are in the range 120°-180° or when one HOCC dihedral angle is from 25°to 100° while the other is from -150° to -180°. An increase in the probability of the HOCC dihedral angle in the range ±120° to ±180° increases the mean dipole moment of EG molecules at high water concentrations.

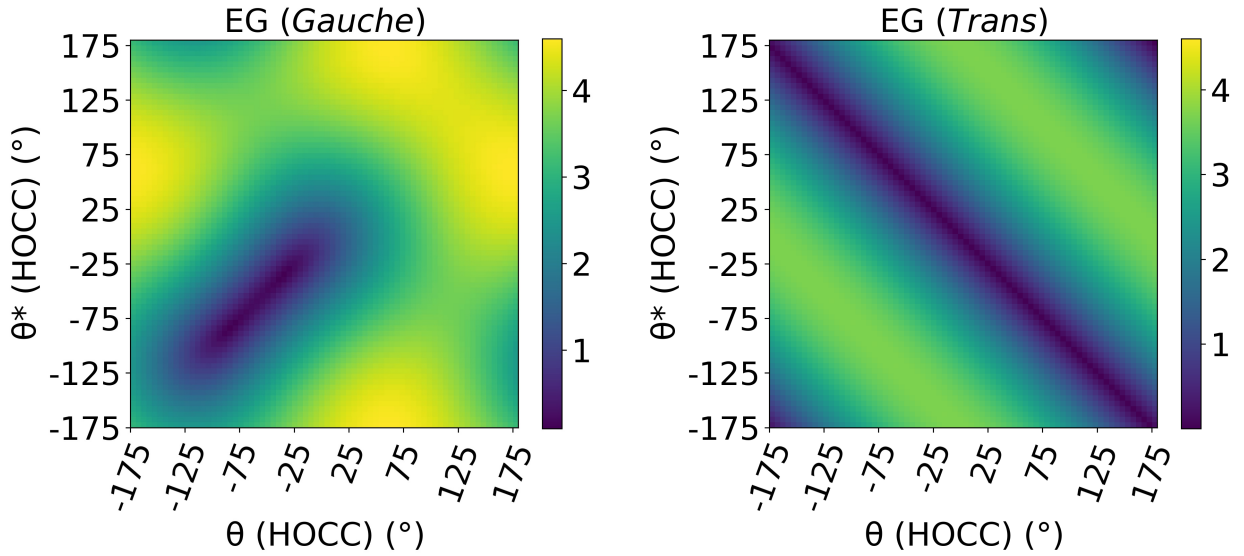

Figure 9: Dipole moment of an isolated EG molecule, calculated using our force field (FF-v1), whose OCCO (central) dihedral angle is 64° (*gauche*) (left panel) and 180° (*trans*) (right panel), as a function of HOCC (terminal) dihedral angles, θ and θ^*. Color bar represents magnitude of dipole moment in Debye.

Conclusions

Both water and ethylene glycol are small molecules and ones whose liquid phases are simple, i.e., homogeneous in both structural and dynamical domains. Yet, their binary mixture solution which spans the entire composition range shows many surprising observations – the clustering of water molecules at low water concentrations, the larger coordination number around water at the equimolar composition, and the fascinating display of conformational selectivity by the organic molecule upon its dilution with water. The current study, employing a bespoke force field for EG, is able to adroitly capture all these key phenomena associated with aqueous EG solution.

The population of EG molecules with their central OCCO dihedral in the *trans* state reduces from a value of 21% in neat liquid EG to a value of around 11% under extremely dilute conditions in water, consistent with several spectroscopic studies and the early quantum chemical work of Cramer and Truhlar.[25] To the best of our knowledge, the current work is the first one to demonstrate the same in an empirical force field based MD simulation. The reduction in the *trans* population with increasing water content is a direct consequence of the increase in the static dielectric constant of the medium, from a value of 41 in neat liquid EG to a value of 78 in neat liquid water. The *trans* fraction observed in dilute EG solution also correlates well with the free energy difference obtained through well tempered metadynamics simulations.

The simulations also offered microscopic insights on the interplay between molecular dipole moments and their conformations. In the solution, the dipole moment distribution of molecules present in their *trans* conformation does not change with solute (EG) concentration, while *gauche* conformers exhibit an additional peak in their dipole moment distribution, at higher moment values, at low EG concentrations. A careful analysis on the origin of this peak leads us to conclude that it arises when both the terminal HOCC dihedrals are around 120-170^o. Such a conformation makes the EG molecule most extended, leading it to acquire larger dipole moment values, as a response to the enhanced static dielectric constant of the

solution, upon dilution with water.

The current work is a demonstration of how the mixture of two fully miscible, simple liquids leads to the emergence of rich phenomena that can be explored through careful molecular simulations. We hope to explore more aspects of such solutions containing ethylene glycol in our future endeavours.

Acknowledgements

We gratefully acknowledge the support and the resources provided by 'PARAM Yukti Facility' under the National Supercomputing Mission, Government of India at the Jawaharlal Nehru Centre For Advanced Scientific Research.

Conflict of interest

The authors declare no conflict of interest.

References

(1) Conrad, F. H.; Hill, E. F.; Ballman, E. A. Freezing Points of the System Ethylene Glycol–Methanol–Water. *Ind. Eng. Chem.* **1940**, *32*, 542–543.

(2) Ott, J. B.; Goates, J. R.; Lamb, J. D. Solid-liquid phase equilibria in water + ethylene glycol. *J. Chem. Thermodyn.* **1972**, *4*, 123–126.

(3) Shimoaka, T.; Hasegawa, T. Molecular structural analysis of hydrated ethylene glycol accounting for the antifreeze effect by using infrared attenuated total reflection spectroscopy. *J. Mol. Liq.* **2016**, *223*, 621–627.

(4) Seiler, J.; Hackmann, J.; Lanzerath, F.; Bardow, A. Refrigeration below zero °C:

Adsorption chillers using water with ethylene glycol as antifreeze. *Int. J. Refrig.* **2017**, *77*, 39–47.

(5) Cordray, D. R.; Kaplan, L. R.; Woyciesjes, P. M.; Kozak, T. F. Solid - liquid phase diagram for ethylene glycol + water. *Fluid Ph. Equilibria* **1996**, *117*, 146–152, Proceedings of the Seventh International Conference on Fluid Properties and Phase Equilibria for Chemical Process Design.

(6) Wang, Y.; Li, F.; Fang, W.; Sun, C.; Men, Z. Study of hydrogen bonding interactions in ethylene glycol-water binary solutions by Raman spectroscopy. *Spectrochim Acta A Mol. Biomol. Spectrosc.* **2021**, *260*, 119916.

(7) Guo, Y.-C.; Cai, C.; Zhang, Y.-H. Observation of conformational changes in ethylene glycol–water complexes by FTIR–ATR spectroscopy and computational studies. *AIP Adv.* **2018**, *8*, 055308.

(8) Chen, Y.; Ozaki, Y.; Czarnecki, M. A. Molecular structure and hydrogen bonding in pure liquid ethylene glycol and ethylene glycol–water mixtures studied using NIR spectroscopy. *Phys. Chem. Chem. Phys.* **2013**, *15*, 18694–18701.

(9) Hommel, E. L.; Merle, J. K.; Ma, G.; Hadad, C. M.; Allen, H. C. Spectroscopic and Computational Studies of Aqueous Ethylene Glycol Solution Surfaces. *J. Phy. Chem. B* **2005**, *109*, 811–818, PMID: 16866446.

(10) Matsugami, M.; Takamuku, T.; Otomo, T.; Yamaguchi, T. Thermal Properties and Mixing State of Ethylene Glycol-Water Binary Solutions by Calorimetry, Large-Angle X-ray Scattering, and Small-Angle Neutron Scattering. *The Journal of Physical Chemistry B* **2006**, *110*, 12372–12379, PMID: 16800561.

(11) Jindal, A.; Vasudevan, S. Conformation of Ethylene Glycol in the Liquid State: Intra- versus Intermolecular Interactions. *J. Phys. Chem. B* **2017**, *121*, 5595–5600, PMID: 28490176.

(12) Howard, D. L.; Jørgensen, P.; Kjaergaard, H. G. Weak Intramolecular Interactions in Ethylene Glycol Identified by Vapor Phase OH-Stretching Overtone Spectroscopy. *J. Am. Chem. Soc.* **2005**, *127*, 17096–17103, PMID: 16316257.

(13) Das, P.; Das, P. K.; Arunan, E. Conformational Stability and Intramolecular Hydrogen Bonding in 1,2-Ethanediol and 1,4-Butanediol. *J. Phy. Chem. A* **2015**, *119*, 3710–3720, PMID: 25839224.

(14) Chopra, D.; Guru Row, T. N.; Arunan, E.; Klein, R. A. Crystalline ethane-1,2-diol does not have intra-molecular hydrogen bonding: Experimental and theoretical charge density studies. *J. Mol. Liq.* **2010**, *964*, 126–133.

(15) Pachler, K.; Wessels, P. Rotational isomerism: X. A nuclear magnetic resonance study of 2-fluoro-ethanol and ethylene glycol. *J. Mol. Struct.* **1970**, *6*, 471–478.

(16) Gaur, A.; Balasubramanian, S. Liquid ethylene glycol: prediction of physical properties, conformer population and interfacial enrichment with a refined non-polarizable force field. *Phys. Chem. Chem. Phys.* **2022**, *24*, 10985–10992.

(17) Zhang, N.; Li, M.-R.; Zhang, F.-S. Structure and dynamics properties of liquid ethylene glycol from molecular dynamics simulations. *Chem. Phys. Lett.* **2019**, *718*, 12–21.

(18) Kaiser, A.; Ritter, M.; Nazmutdinov, R.; Probst, M. Hydrogen Bonding and Dielectric Spectra of Ethylene Glycol–Water Mixtures from Molecular Dynamics Simulations. *J. Phy. Chem. B* **2016**, *120*, 10515–10523, PMID: 27649083.

(19) Antipova, M. L.; Gurina, D. L.; Makarov, D. M.; Egorov, G. I.; Petrenko, V. E. Effect of pressure on the structure and dynamics of hydrogen bonds in ethylene glycol–water mixtures: Numerical simulation data. *Russ. J. Phys. Chem. A* **2016**, *90*, 560–566.

(20) Vital de Oliveira, O.; Gomide Freitas, L. C. Molecular dynamics simulation of liquid ethylene glycol and its aqueous solution. *J. Mol. Struct. Theochem* **2005**, *728*, 179–187.

(21) Gubskaya, A. V.; Kusalik, P. G. Molecular Dynamics Simulation Study of Ethylene Glycol, Ethylenediamine, and 2-Aminoethanol. 2. Structure in Aqueous Solutions. *J. Phy. Chem. A* **2004**, *108*, 7165–7178.

(22) Kumar, R. M.; Baskar, P.; Balamurugan, K.; Das, S.; Subramanian, V. On the Perturbation of the H-Bonding Interaction in Ethylene Glycol Clusters upon Hydration. *J. Phy. Chem. A* **2012**, *116*, 4239–4247, PMID: 22530594.

(23) Geerke, D. P.; van Gunsteren, W. F. The performance of non-polarizable and polarizable force-field parameter sets for ethylene glycol in molecular dynamics simulations of the pure liquid and its aqueous mixtures. *Molecular Physics* **2007**, *105*, 1861–1881.

(24) Chaudhari, A.; Lee, S.-L. A computational study of microsolvation effect on ethylene glycol by density functional method. *J. Chem. Phys.* **2004**, *120*, 7464–7469.

(25) Cramer, C. J.; Truhlar, D. G. Quantum Chemical Conformational Analysis of 1,2-Ethanediol: Correlation and Solvation Effects on the Tendency To Form Internal Hydrogen Bonds in the Gas Phase and in Aqueous Solution. *J. Am. Chem. Soc.* **1994**, *116*, 3892–3900.

(26) Jorgensen, W. L. Optimized intermolecular potential functions for liquid alcohols. *J. Phys. Chem.* **1986**, *90*, 1276–1284.

(27) Wang, J.; Wolf, R. M.; Caldwell, J. W.; Kollman, P. A.; Case, D. A. Development and testing of a general amber force field. *J. Comput. Chem.* **2004**, *25*, 1157–1174.

(28) H.J.C., B.; D., v.; R., v. GROMACS: A message-passing parallel molecular dynamics implementation. *Comput. Phys. Commun.* **1995**, *91*, 43–56.

(29) Abraham, M. J.; Murtola, T.; Schulz, R.; Páll, S.; Smith, J. C.; Hess, B.; Lindahl, E. GROMACS: High performance molecular simulations through multi-level parallelism from laptops to supercomputers. *SoftwareX* **2015**, *1-2*, 19–25.

(30) Lindahl, E.; Abraham, M. J.; Hess, B.; D., v. GROMACS 2020.1 Source code (2020.1). Zenodo. **2020**,

(31) Martínez, L.; Andrade, R.; Birgin, E. G.; Martínez, J. M. PACKMOL: A package for building initial configurations for molecular dynamics simulations. *J. Comput. Chem.* **2009**, *30*, 2157–2164.

(32) Berendsen, H. J. C.; Grigera, J. R.; Straatsma, T. P. The missing term in effective pair potentials. *J. Phys. Chem.* **1987**, *91*, 6269–6271.

(33) Páll, S.; Hess, B. A flexible algorithm for calculating pair interactions on SIMD architectures. *Comput. Phys. Commun.* **2013**, *184*, 2641–2650.

(34) Essmann, U.; Perera, L.; Berkowitz, M. L.; Darden, T.; Lee, H.; Pedersen, L. G. A smooth particle mesh Ewald method. *J. Chem. Phys.* **1995**, *103*, 8577–8593.

(35) Hess, B.; Bekker, H.; Berendsen, H. J. C.; Fraaije, J. G. E. M. LINCS: A linear constraint solver for molecular simulations. *J. Comput. Chem.* **1997**, *18*, 1463–1472.

(36) Nosé, S. A unified formulation of the constant temperature molecular dynamics methods. *J. Chem. Phys.* **1984**, *81*, 511–519.

(37) Nosé, S. A molecular dynamics method for simulations in the canonical ensemble. *Mol. Phys.* **1984**, *52*, 255–268.

(38) Parrinello, M.; Rahman, A. Polymorphic transitions in single crystals: A new molecular dynamics method. *J. Appl. Phys.* **1981**, *52*, 7182–7190.

(39) Tribello, G. A.; Bonomi, M.; Branduardi, D.; Camilloni, C.; Bussi, G. PLUMED 2: New feathers for an old bird. *Comput. Phys. Commun.* **2014**, *185*, 604–613.

(40) Barducci, A.; Bussi, G.; Parrinello, M. Well-Tempered Metadynamics: A Smoothly Converging and Tunable Free-Energy Method. *Phys. Rev. Lett.* **2008**, *100*, 020603.

(41) Sun, T.; Teja, A. S. Density, Viscosity, and Thermal Conductivity of Aqueous Ethylene, Diethylene, and Triethylene Glycol Mixtures between 290 K and 450 K. *J. Chem. Eng. Data* **2003**, *48*, 198–202.

(42) Ambrosone, L.; D'Errico, G.; Sartorio, R.; Costantino, L. Dynamic properties of aqueous solutions of ethylene glycol oligomers as measured by the pulsed gradient spin-echo NMR technique at 25[deg]C. *J. Chem. Soc., Faraday Trans.* **1997**, *93*, 3961–3966.

(43) Zagrebin, P. A.; Buchner, R.; Nazmutdinov, R. R.; Tsirlina, G. A. Dynamic Solvent Effects in Electrochemical Kinetics: Indications for a Switch of the Relevant Solvent Mode. *J. Phy. Chem. B* **2010**, *114*, 311–320, PMID: 20000826.

(44) Loskutov, V. V.; Kosova, G. N. Molecular Structure of an Ethylene Glycol–Water Solution at 298 K. *Russian Journal of Physical Chemistry A* **2019**, *93*, 260–264.

(45) Ning, F. L.; Glavatskiy, K.; Ji, Z.; Kjelstrup, S.; H. Vlugt, T. J. Compressibility, thermal expansion coefficient and heat capacity of CH4 and CO2 hydrate mixtures using molecular dynamics simulations. *Phys. Chem. Chem. Phys.* **2015**, *17*, 2869–2883.

(46) Kaur, S.; Shobhna,; Kashyap, H. K. Insights Gained from Refined Force-Field for Pure and Aqueous Ethylene Glycol through Molecular Dynamics Simulations. *The Journal of Physical Chemistry B* **2019**, *123*, 6543–6553, PMID: 31335141.

(47) Jerie, K.; Baranowski, A.; Przybylski, J.; Glinski, J. Ultrasonic and positron annihilation studies of liquid solutions of n-hexanol in 1,2-ethanediol. *Journal of Molecular Liquids* **2004**, *111*, 25–31.

(48) Washburn, E. W.; West, C. J.; Dorsey, N. E. *International critical tables of numerical data, physics, chemistry, and technology*; Knovel: Norwich, New York, 2003.

(49) Yang, C.; Ma, P.; Jing, F.; Tang, D. Excess Molar Volumes, Viscosities, and Heat

Capacities for the Mixtures of Ethylene Glycol + Water from 273.15 K to 353.15 K. *J. Chem. Eng. Data* **2003**, *48*, 836–840.

(50) Fortes, A. D.; Suard, E. Crystal structures of ethylene glycol and ethylene glycol monohydrate. *J. Chem. Phys.* **2011**, *135*, 234501.

(51) Jindal, A.; Vasudevan, S. Ethylene Glycol Dihedral Angle Dynamics: Relating Molecular Conformation to the Raman Spectrum of the Liquid. *J. Phy. Chem. B* **2021**, *125*, 1888–1895, PMID: 33560860.

Table of Contents

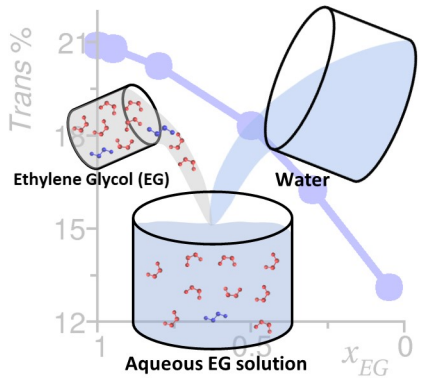

Figure 10: Table of Content Graphics.

The fraction of ethylene glycol molecules with their central OCCO dihedral in *gauche* conformation increases from 79% in the neat liquid to 89% when it is diluted with water.

Supporting Information for: Conformer Selection Upon Dilution with Water: The Fascinating Case of Liquid Ethylene Glycol Studied via Molecular Dynamics Simulations

Anjali Gaur and Sundaram Balasubramanian*

Chemistry and Physics of Materials Unit

Jawaharlal Nehru Centre for Advanced Scientific Research, Bangalore 560 064, India

E-mail: bala@jncasr.ac.in

Contents

S1 Nomenclature

S1.1 Ethylene Glycol Conformation

The molecular structure of ethylene glycol (EG) is shown in Figure S1. An EG molecule has one central dihedral angle (O-C-C-O) and two terminal dihedral angles (H-O-C-C). The nomenclature of an EG molecule is based on its dihedral angle values. If a dihedral angle is between ±150 degree, and ±180 degree it is termed as *trans* (t/T) and if the range is between ±30 to ±90 degree, it is termed as *gauche* (g/G). Upper case T and G are used for the OCCO dihedral angle while lower case t and g are used for clockwise rotated HOCC dihedrals and t' and g' for anticlockwise rotated HOCC dihedrals. In this paper, our main focus is on the central OCCO dihedral angle, hence in the paper *trans* and *gauche* EG conformers are referred based on the OCCO dihedral angle.

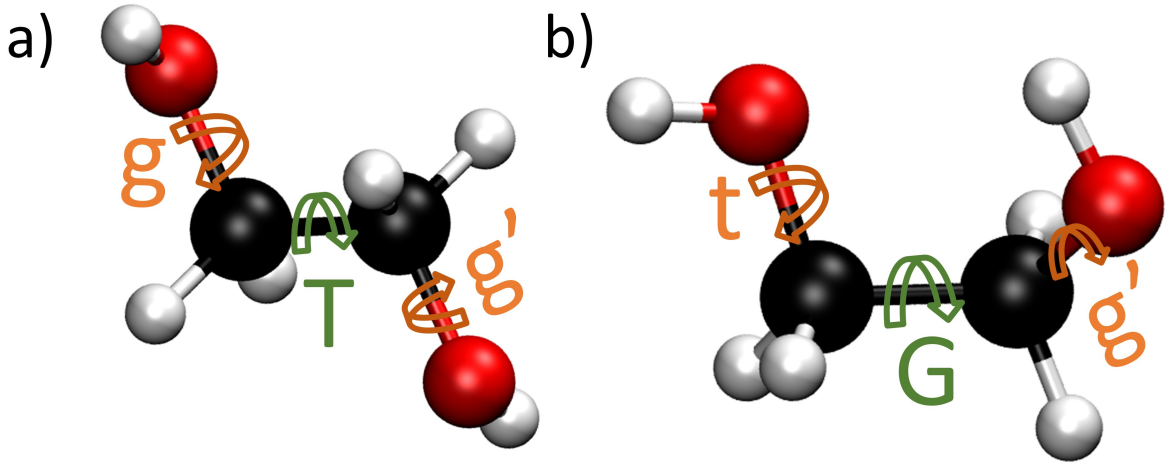

Figure S1: Molecular structure of ethylene glycol molecule a) gTg' conformation and b) tGg' conformation. Color code: H: white, O: red, C: lack.

S1.2 Atom Type

Atom types for EG and water used to perform molecular dynamics simulations are shown in Figure S2.

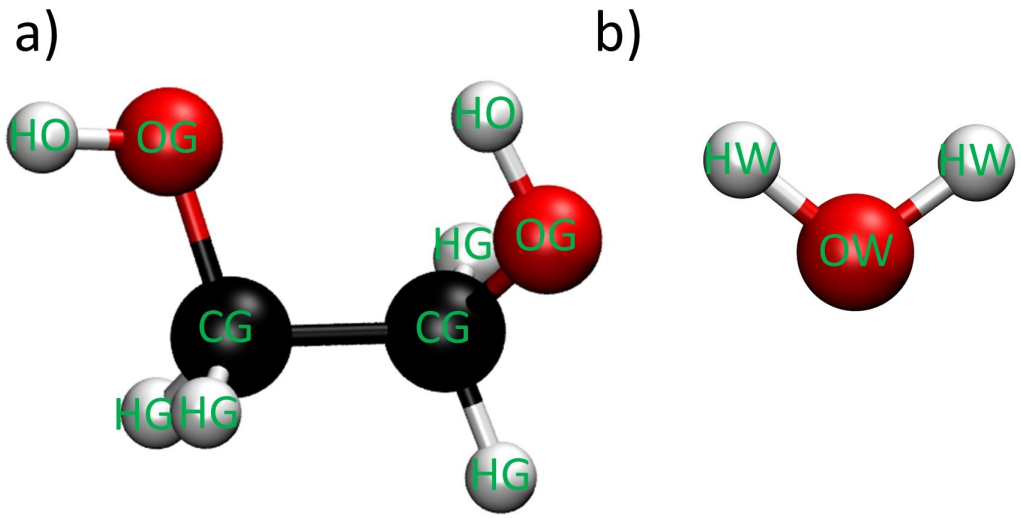

Figure S2: Atom types used in the force field for (a) Ethylene glycol (b) Water.

S2 Simulation System Details

Table S1: Simulation box details for classical MD simulations of ethylene glycol-water binary mixtures at several mole fractions of EG (x_{EG}). The box length reported here is the average box length calculated from the last 5ns of 25ns NPT simulations at 298.15K and 1bar.

x_{EG}	Number of molecules		Cubic box Length (Å)
	EG	Water	
0	0	4500	51.27
0.05	211	4000	51.82
0.30	857	2000	51.86
0.50	1050	1050	50.60
0.80	1280	320	50.63
0.95	1425	75	51.45

S3 Radial Distribution Functions

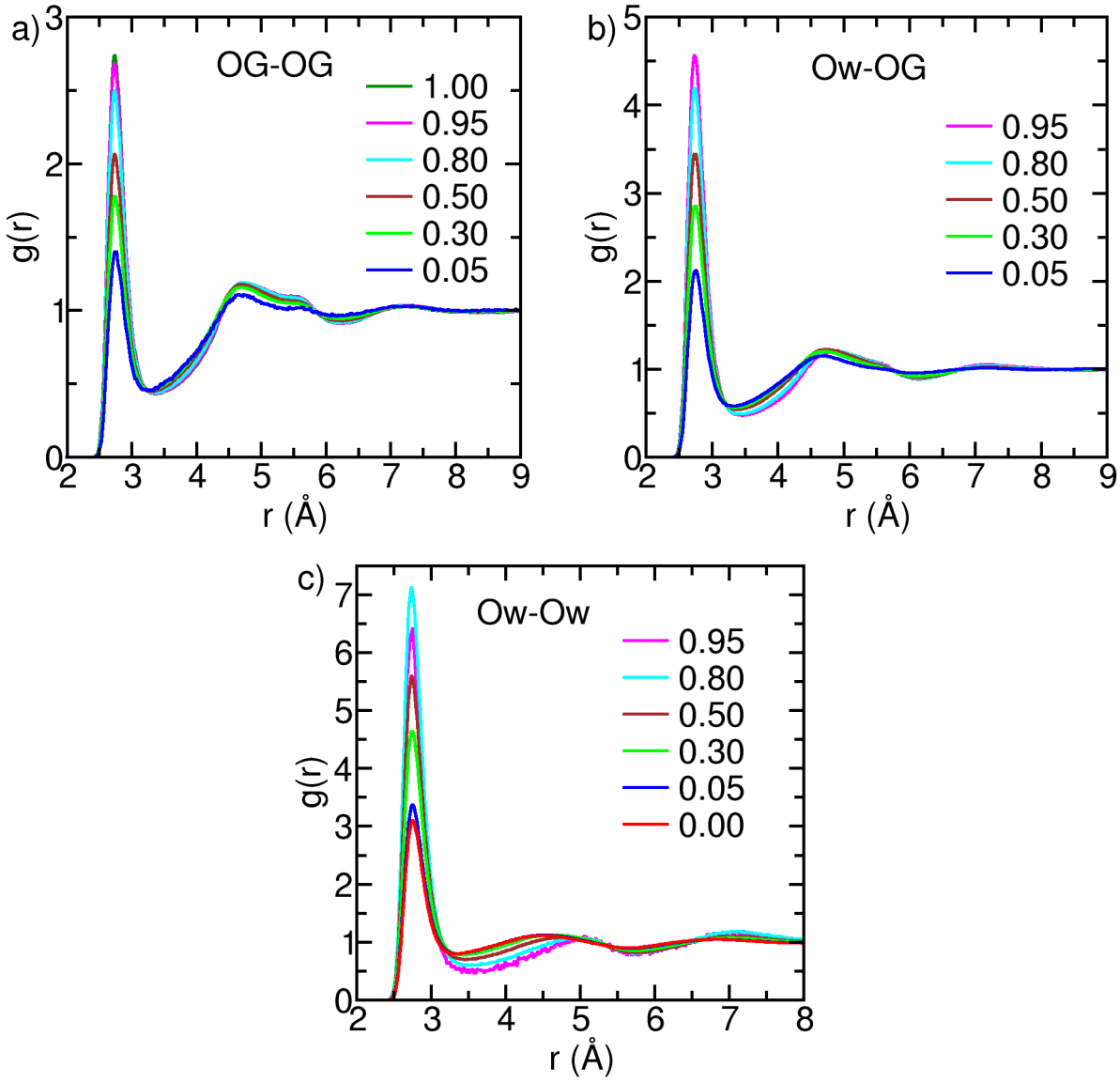

Figure S3: Intermolecular radial distribution function between oxygen atoms of a) EG molecules (OG) b) water molecules (Ow) and EG molecules (OG) c) water molecules (Ow). Legends represent mole fraction of EG.

Table S2: First shell coordination number (C.N.) of oxygen atoms of OG and Ow types around a central oxygen atom of either type, at several mole fractions of EG x_{EG}.

x_{EG}	OG-OG	Ow-OG	OG-Ow	Ow-Ow
1.00	2.23	-	-	-
0.95	2.16	3.50	0.09	0.12
0.80	1.93	3.16	0.39	0.65
0.50	1.32	2.21	1.10	1.77
0.30	0.88	1.44	1.68	2.70
0.05	0.19	0.27	2.60	4.17
0.00	-	-	-	4.41

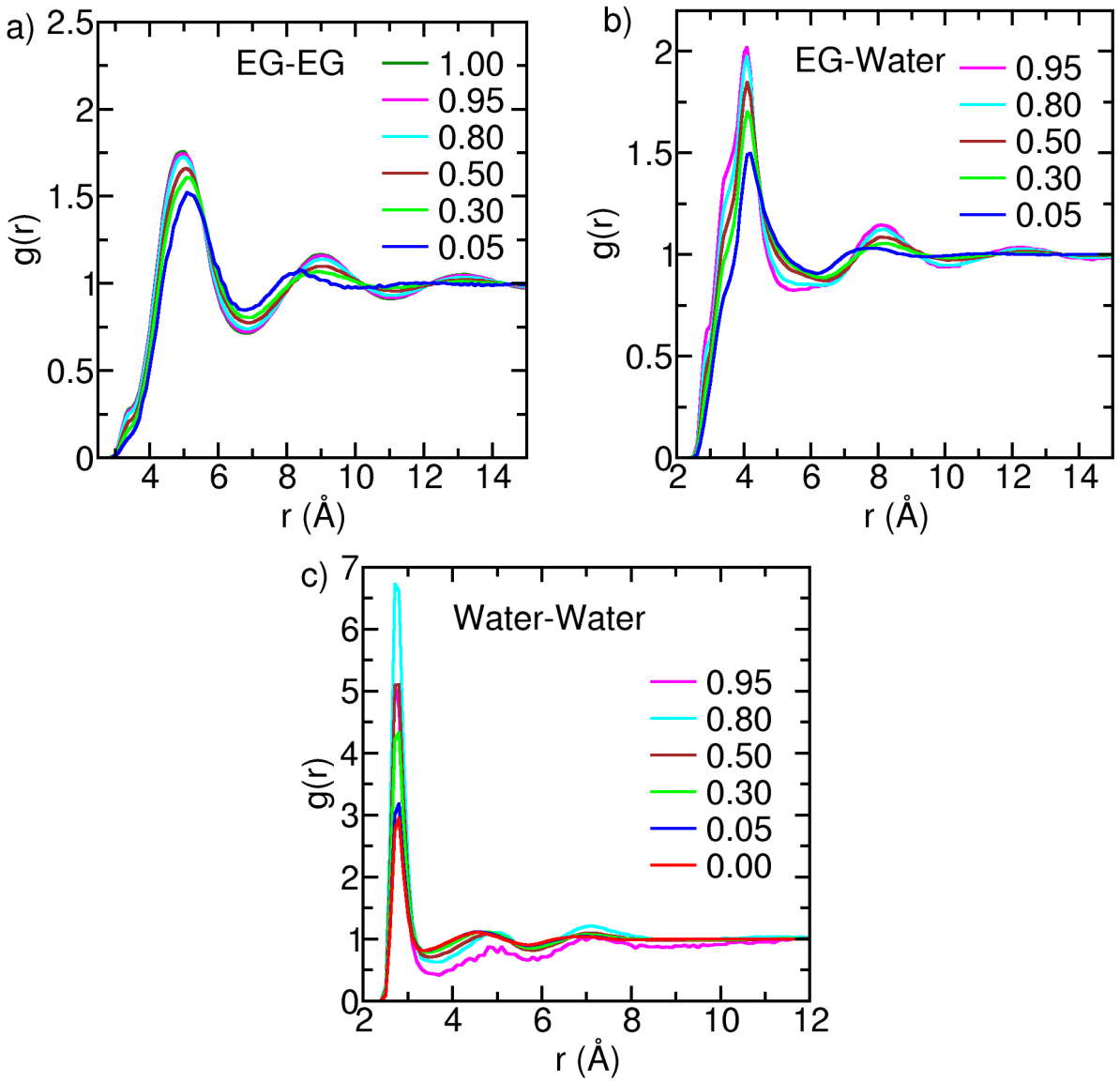

Figure S4: Center of mass radial distribution functions between (a) EG molecules (b) EG and water molecules (c) water molecules. Legends represent mole fraction of EG.

Table S3: First shell coordination number (C.N.) of center of mass of molecules at several mole fractions of EG, x_{EG}.

x_{EG}	EG-EG (6.8-6.9 Å)	Water-EG (6.2-6.5 Å)	EG-Water (6.2-6.5 Å)	Water-Water (3.3-3.7 Å)
1.00	13.93	-	-	-
0.95	13.28	10.10	0.53	0.12
0.80	12.95	10.79	2.70	0.72
0.50	10.59	8.79	8.97	1.82
0.30	7.96	6.43	15.01	2.90
0.05	1.83	1.39	26.45	4.34
0.00	-	-	-	4.37

S4 Density

Table S4: Density of aqueous ethylene glycol solutions at different mole fractions of EG (x_{EG}) at 298.15 K and 1 bar. The density values were calculated from the last 5ns of a 25ns NPT simulation. Experimental data is taken from Ref. 1. The computed densities are within 1.4 % of the experimental values. The error on the mean is calculated by dividing the 5ns trajectory into five segments of 1ns each.

x_{EG}	Expt. Density (kg/m^3)	Simu. Density (kg/m^3)	Deviation (%)
0.00	997.1	998.7 ± 0.05	0.16
0.05	1018.7	1016.2 ± 0.16	-0.25
0.30	1074.2	1062.4 ± 0.41	-1.10
0.50	1092.5	1078.1 ± 0.26	-1.32
0.80	1105.9	1090.4 ± 0.21	-1.40
0.95	1109.8	1094.6 ± 0.64	-1.37
1.00	1110.8	1096.2 ± 0.32	-1.31

S5 Self-diffusion Coefficient

Self-diffusion coefficient was calculated using equation S1 from the mean square dispacement (MSD) of molecules.

$$D_{self} = \frac{1}{6} \lim_{t \to \infty} \frac{d}{dt} \left\langle \frac{1}{N} \sum_{i=1}^{N} (\mathbf{r_i}(t) - \mathbf{r_i}(0))^2 \right\rangle \tag{S1}$$

Where t is time, N is the total number of molecules, $\mathbf{r}$ is the center of mass position of the molecules and angular brackets represent averaging over multiple time origins. β, the exponent in the relation between MSD and time, was calculated using equation S2 to find the diffusive regime. The system is guaranteed to be in diffusive regime when β is equal to unity. MSD versus simulation time and β versus simulation time plots are shown in Figures S5.

$$\beta(t) = \frac{d\, ln(MSD(t))}{d\, ln(t)} \tag{S2}$$

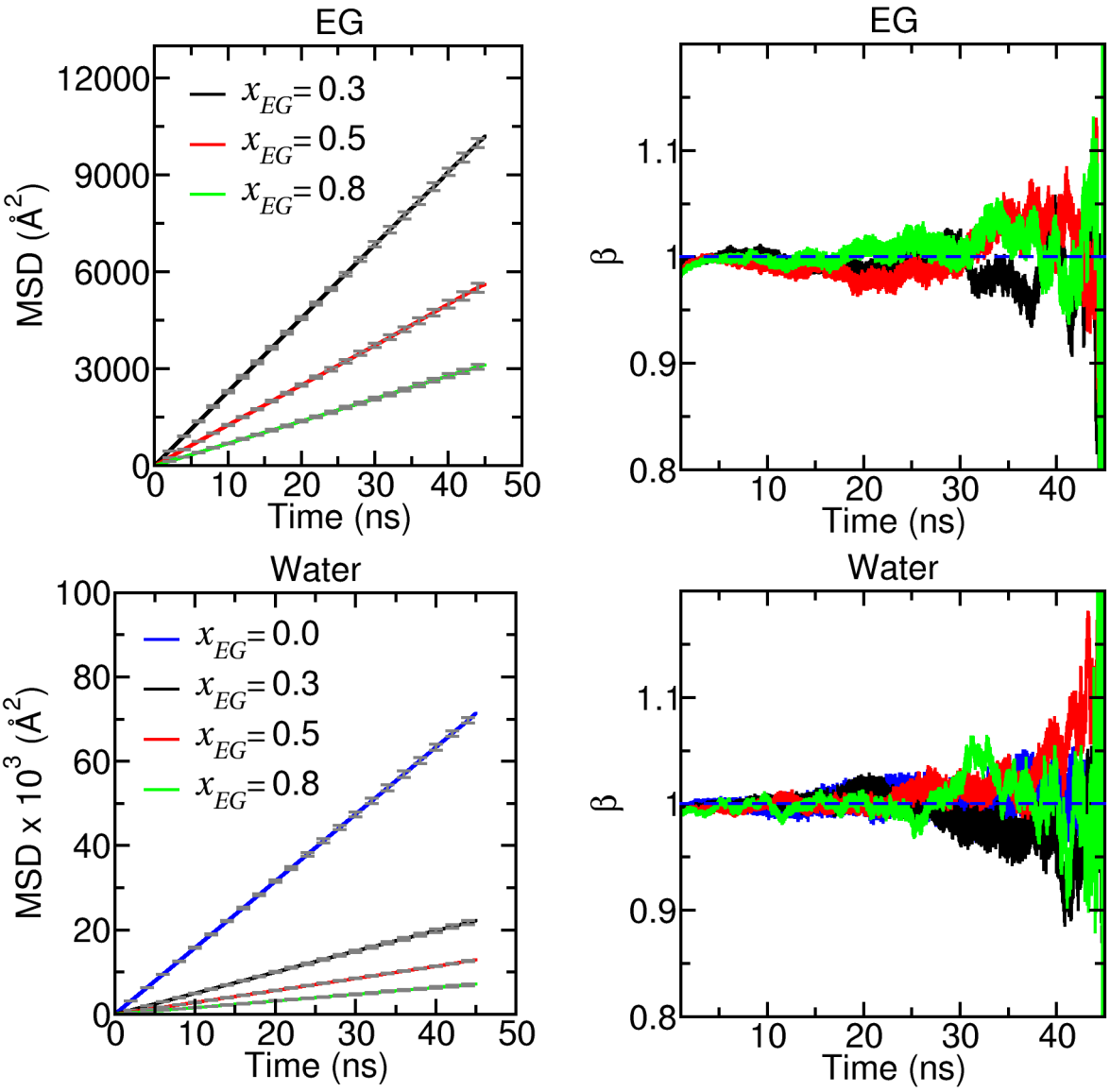

Figure S5: Mean square displacement (MSD) of molecules as a function of simulation time (left) calculated to estimate self-diffusion coefficient. β calculated using equation S2 to find the diffusive regime.

Table S5: Self-diffusion coefficient (D_{self}) values computed at different mole fractions of EG (x_{EG}) at 298.15 K and the average β value in the time interval in which D_{self} is computed. Experimental data is taken from Ref. 2. The uncertainty in computed D_{self} is calculated using the block averaging method (6 blocks, each of 5 ns duration). The computed D_{self} values are within 14.6 % of the experimental values.

Water						
x_{EG}	Time Interval (ns)		Average β	D_{self} (10^{-5} cm^2/s)		Δ D_{self} (%)
	t_{start}	t_{end}		Experimental[2]	This work	
0.00	5	35	1.002	2.299	2.634 ± 0.009	14.57
0.30	5	35	0.997	0.751	0.830 ± 0.008	10.52
0.50	5	35	1.005	0.422	0.473 ± 0.004	12.09
0.80	5	35	1.004	0.300	0.265 ± 0.004	-11.67
EG						
x_{EG}	Time Interval (ns)		Average β	D_{self} (10^{-5} cm^2/s)		Δ D (%)
	t_{start}	t_{end}		Experimental[2]	This work	
0.30	5	35	0.995	0.359	0.379 ± 0.008	5.57
0.50	5	35	0.992	0.207	0.207 ± 0.003	0.00
0.80	5	35	1.006	0.116	0.116 ± 0.001	0.00

S6 Dielectric Constant

GROMACS-2020.4[3] patched with PLUMED-2.6.2[4] was used to write the total dipole moment of the simulation box ($\overrightarrow{M}$) every 1 fs. The static dielectric constant was calculated using fluctuations in $\overrightarrow{M}$[5] using equation S3.

$$\epsilon = 1 + \frac{4\pi}{3\epsilon_0 k_B T V}(\langle \overrightarrow{M}^2 \rangle - \langle \overrightarrow{M} \rangle^2) \tag{S3}$$

Cumulative running averages of static dielectric constant calculated from the six independent NVT simulations are shown in Figures S6 and S7. Each simulation was run for 50 ns. The dielectric constant approaches convergence in 30 ns.

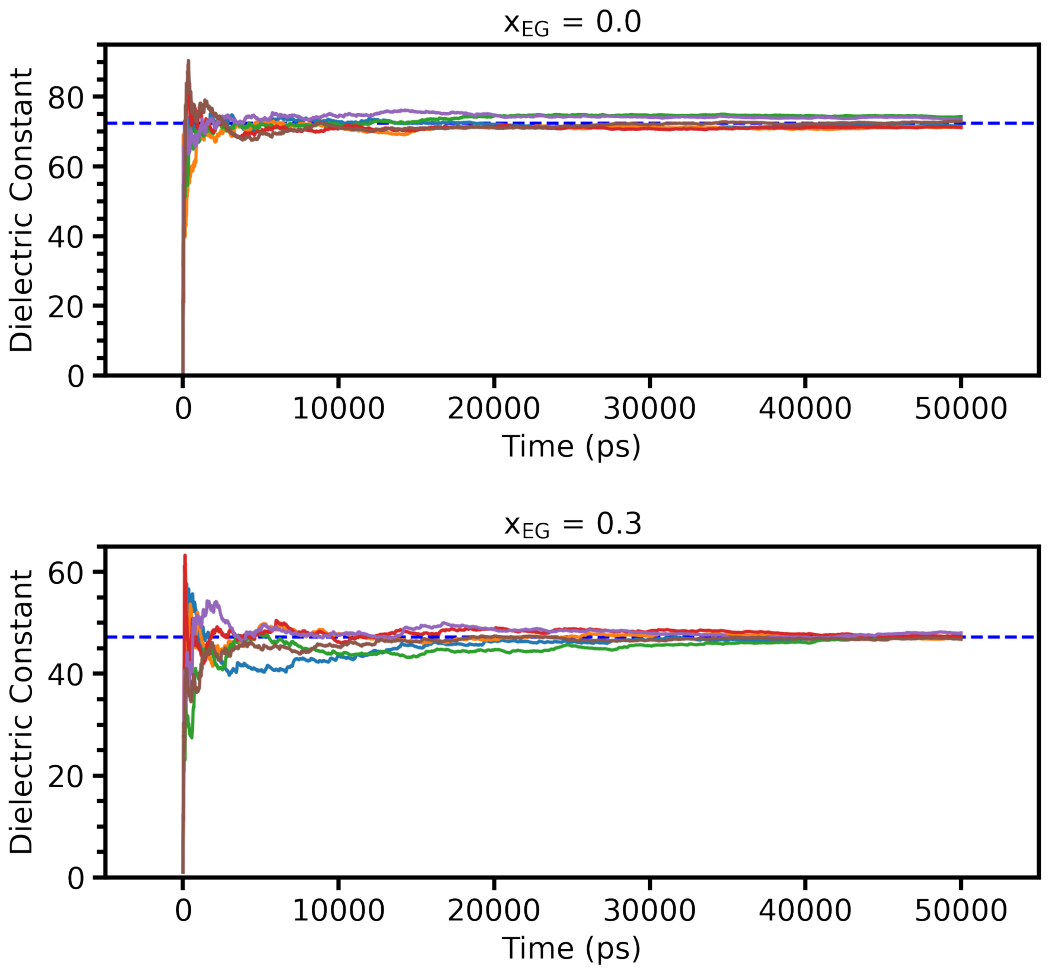

Figure S6: Running average of static dielectric constant as a function of simulation time for EG mole fraction (x_{EG}) of 0.0 and 0.3. The dashed line represent mean dielectric constant calculated from six independent runs.

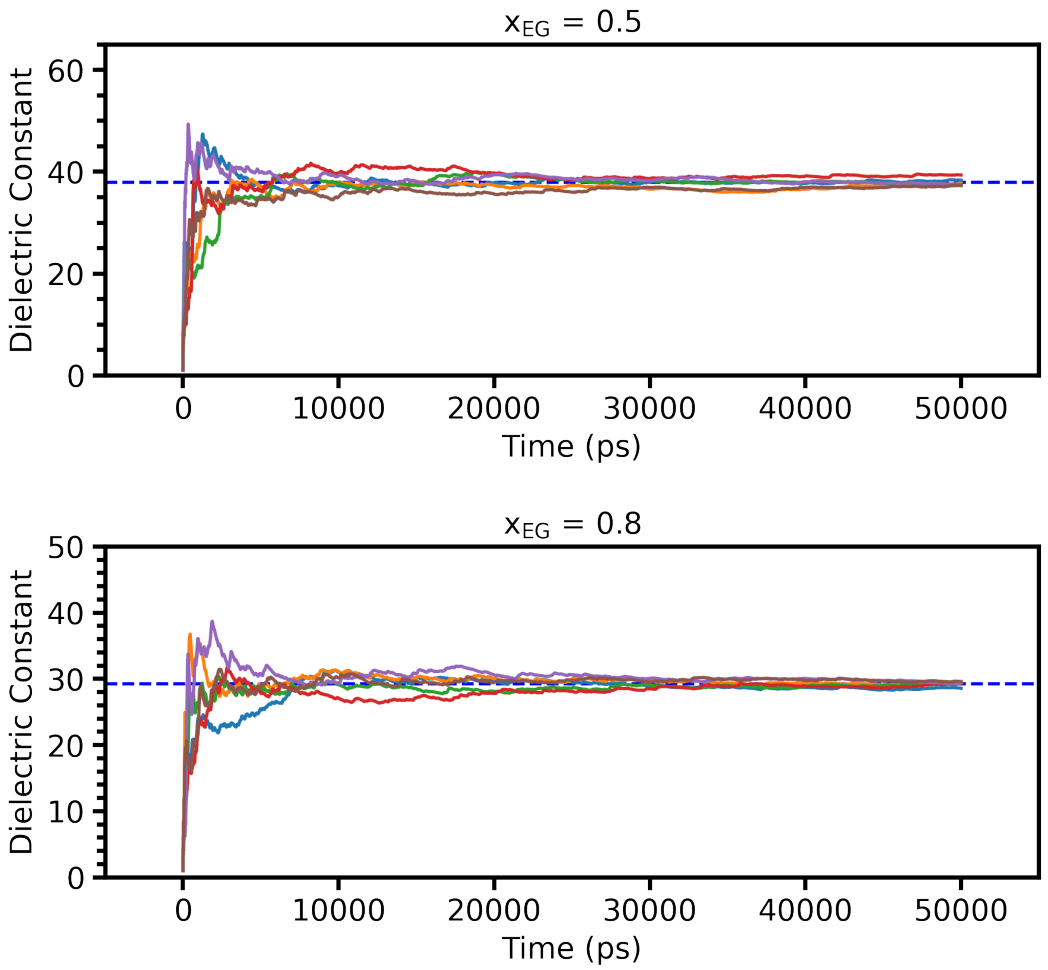

Figure S7: Running average of static dielectric constant as a function of simulation time for EG mole fraction (x_{EG}) of 0.5 and 0.8. The dashed line represent mean dielectric constant calculated from six independent runs.

Table S6: Static dielectric constant values computed at different mole fractions of EG (x_{EG}) at 298.15 K by averaging over six independent simulations. Experimental data is taken from Ref. 6. A maximum deviation from experimental data is -35.53 % at $x_{EG} = 1.0$.

x_{EG}	Dielectric Constant		Deviation (%)
	Experimental[6]	This work	
0.00	78.17	72.45 ± 1.21	-7.32
0.30	60.22	47.24 ± 0.42	-21.55
0.50	52.75	37.94 ± 0.73	-28.08
0.80	44.59	29.29 ± 0.35	-34.31
1.00	40.70	29.24 ± 0.54	-35.53

S7 Well-tempered Metadynamics

Table S7: Simulation box details for well-tempered metadynamics simulation. The box length reported here is the mean calculated over the last 5ns of 25ns NPT simulations at 298.15K and 1bar.

Number of molecules		Cubic box Length (Å)
EG	Water	
1	4496	51.27

Table S8: Simulation parameters for WTMetaD simulation performed at 298.15 K.

Gaussian width	Initial Gaussian Height	Bias Deposition Rate	Bias factor
20.05 °	0.3 kJ/mol	0.5 ps	6

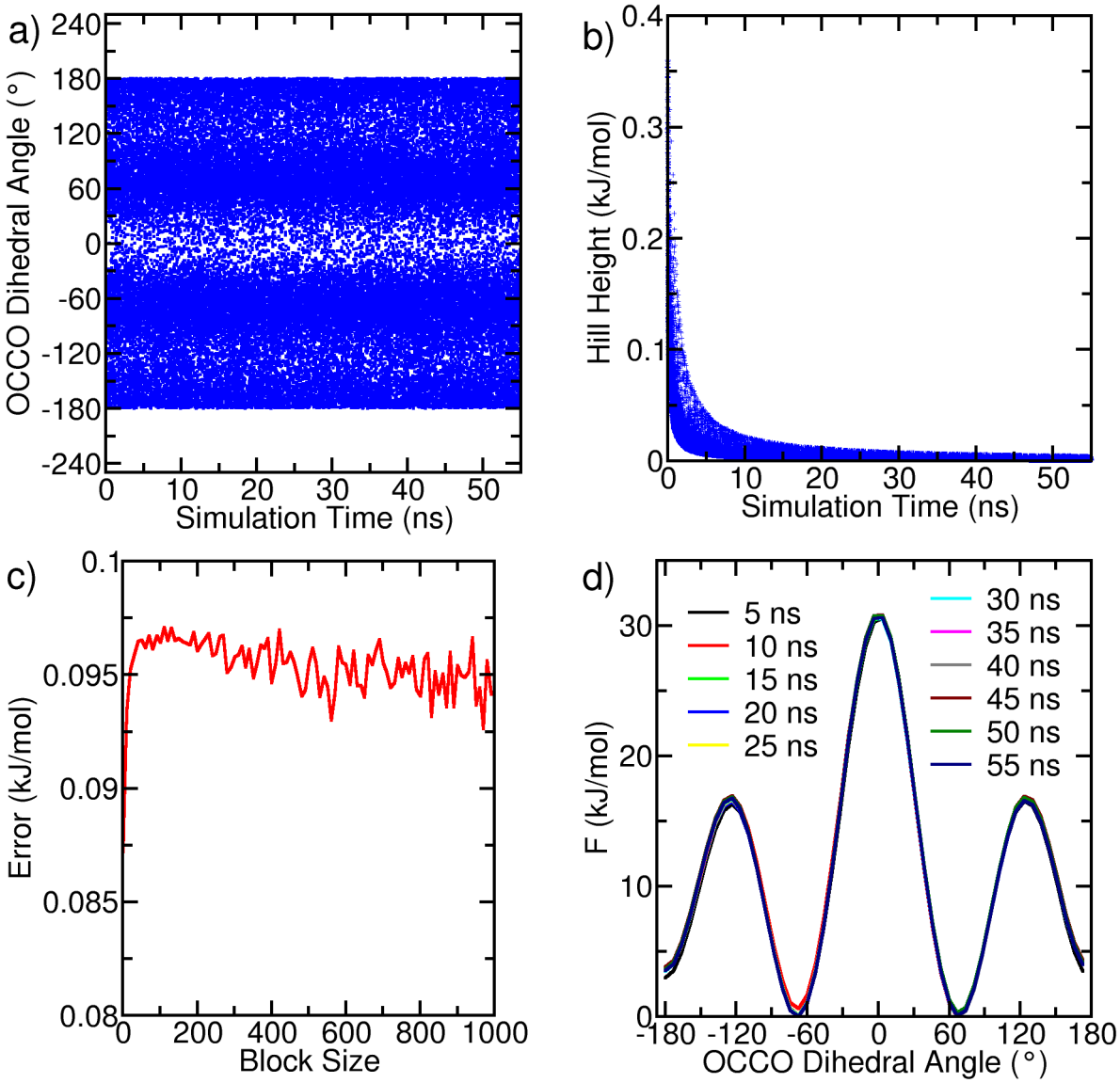

Figure S8: a) OCCO dihedral angle as a function of WTMetaD simulation time. b) Gaussian hill height as a function of simulation time, the hill height approached a value of zero. c) Error calculated with respect to block size. Maximum error in free energy is 0.097 kJ/mol. d) Free energy profile calculated after every 5ns.

S8 Dihedral Distribution

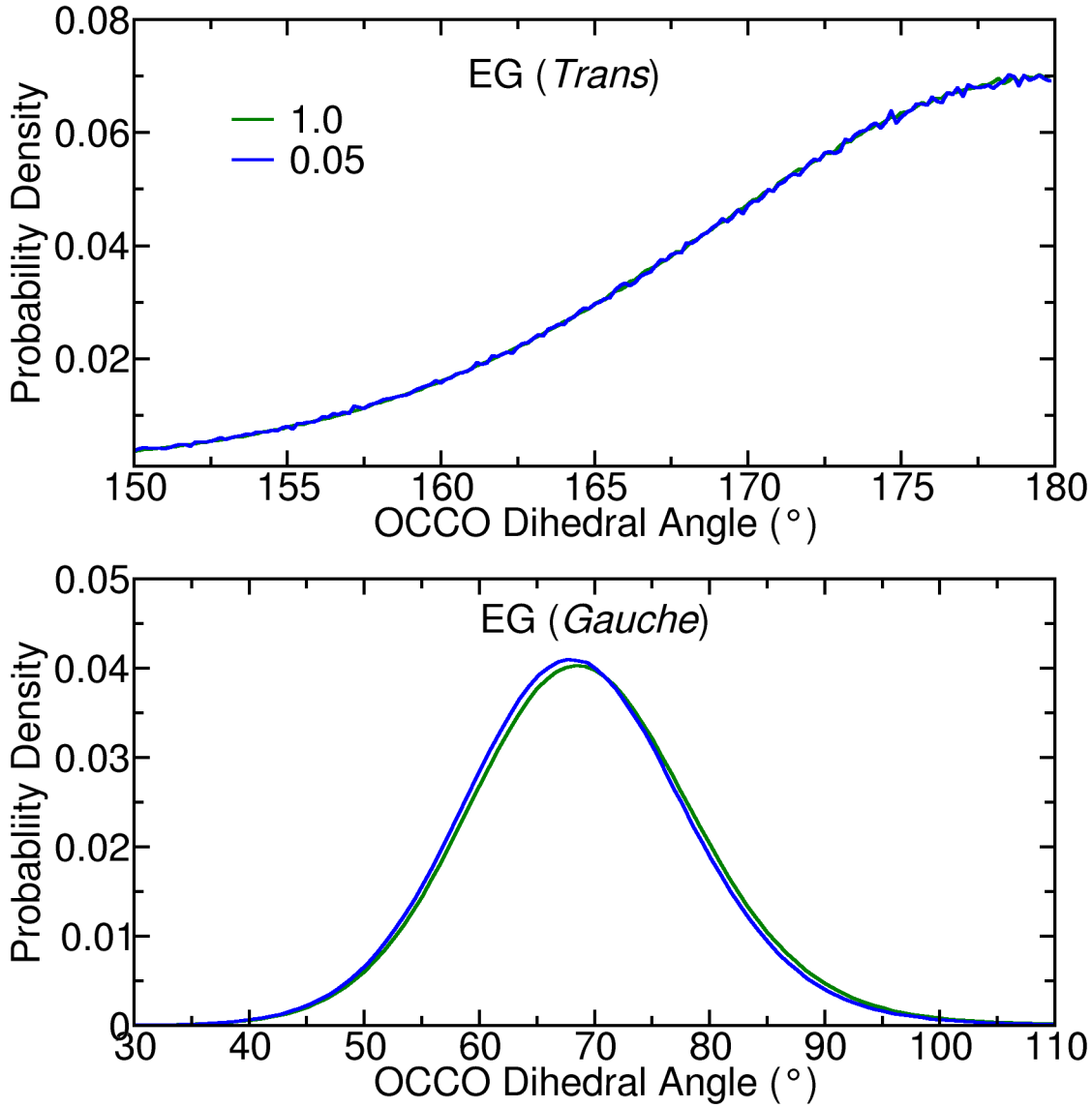

Figure S9: Central OCCO dihedral distribution of EG molecules in *gauche* (top) and *trans* (bottom) conformations.

References

(1) Sun, T.; Teja, A. S. Density, Viscosity, and Thermal Conductivity of Aqueous Ethylene, Diethylene, and Triethylene Glycol Mixtures between 290 K and 450 K. *J. Chem. Eng. Data* **2003**, *48*, 198–202.

(2) Ambrosone, L.; D'Errico, G.; Sartorio, R.; Costantino, L. Dynamic properties of aqueous solutions of ethylene glycol oligomers as measured by the pulsed gradient spin-echo NMR technique at 25[deg]C. *J. Chem. Soc., Faraday Trans.* **1997**, *93*, 3961–3966.

(3) Lindahl, E.; Abraham, M. J.; Hess, B.; D., v. GROMACS 2020.1 Source code (2020.1). Zenodo. **2020**,

(4) Tribello, G. A.; Bonomi, M.; Branduardi, D.; Camilloni, C.; Bussi, G. PLUMED 2: New feathers for an old bird. *Comput. Phys. Commun.* **2014**, *185*, 604–613.

(5) Gereben, O.; Pusztai, L. On the accurate calculation of the dielectric constant from molecular dynamics simulations: The case of SPC/E and SWM4-DP water. *Chemical Physics Letters* **2011**, *507*, 80–83.

(6) Zagrebin, P. A.; Buchner, R.; Nazmutdinov, R. R.; Tsirlina, G. A. Dynamic Solvent Effects in Electrochemical Kinetics: Indications for a Switch of the Relevant Solvent Mode. *J. Phy. Chem. B* **2010**, *114*, 311–320, PMID: 20000826.